Applied Surface Science 628 (2023) 157315

Contents lists available at ScienceDirect

Applied Surface Science

journal homepage: www.elsevier.com/locate/apsusc

Full Length Article

Fe_4 cluster as the smallest 3D Fe cluster with unique quantum magnetic levitation effect on graphene

Ning-Gui Ma [a,b,c,e], Yong-Jia Zhang [b], He-Na Zhang [c], Hui-Min Mu [c], Yong Zhang [d,*], Xiao-Chun Wang [a,c,*]

[a] School of Physics Science and Information Technology, Liaocheng University, Liaocheng 252000, China
[b] College of Physics and Optoelectronics, Taiyuan University of Technology, Taiyuan 030024, China
[c] Institute of Atomic and Molecular Physics, Jilin University, Changchun 130012, China
[d] Department of Electrical and Computer Engineering, The University of North Carolina at Charlotte, Charlotte, NC 28223-0001, USA
[e] Department of Materials Science and Engineering, City University of Hong Kong, Hong Kong, China

ARTICLE INFO

Keywords:
First-principles calculations
Two-dimensional diamagnetism
Spontaneous quantum magnetic levitation
Extremely-high density independent quantum dots

ABSTRACT

The unique quantum magnetic levitation effect of small metallic clusters adsorbed on graphene has been studied for their minimal energy configurations in this work. Using first-principles calculations, we specially focus on the tetrahedral Fe_4 clusters in a corn-like configuration for the induced magnetic moments in the Fe_4 cluster and graphene. Firstly, the 3D magnetic Fe_4 cluster spontaneously induced a diamagnetic moment in graphene in the absence of external energy injection. Additionally, as the smallest 3D particle (among Fe_n clusters), the Fe_4 cluster can be levitated by the repulsive magnetic interaction between the Fe cluster and graphene. The maximum energy barrier between different adsorption configurations of the Fe_4 cluster on graphene is as low as 0.8 eV, making the Fe_4 cluster diffusible between sites with a minimal external force. The conversion energy barrier is relatively low, resulting in low energy consumption. Importantly, the repulsion between Fe clusters may lead to the formation of an ultrahigh-density ($1.18 \times 10^{14}/cm^2$) isolated quantum dot array and avoids the formation of larger clusters. These quantum states might be usable for nanoscale data storage devices for next-generation computing applications, and the small diffusion barrier might offer potential applications in quantum mechanical sensing and nanoscale magnetic levitation.

1. Introduction

The unique two-dimensional structure of graphene makes its surface easy to adsorb various molecules or atoms, providing a template to achieve new functionalities [1–7]. For example, the magnetization of graphene can be changed by adsorbing functional atoms, e.g., H, Co, Ni, V or Fe [8,9]. The results of scanning tunneling microscopy and first-principles calculation have shown that different metal atoms adsorbed on graphene may adopt various configurations with different adsorption energies [9–12]. In addition to alkali and simple metals [13–16], the adsorption of transition metals on graphene has been extensively studied [17–23]. The charge transfer induced by metal atom adsorption can lead to changes in the magnetic properties of the system [9]. Compared with other metals, Fe atoms on graphene are more interesting, since not only the magnetism of Fe_n cluster is retained in Fe_n/graphene system, but also the increasing of magnetic moment of Fe_n/graphene system as the number of Fe atom raises because of the forming of the electric dipole–dipole interactions [9,24,25]. Generally, the application of graphene in spintronics must include a ferromagnetic spin injector [26]. Magnetism can be induced in graphene by doping it with transition metals, which has great potential in spintronics [27,28]. Furthermore, Fe adatoms tend to form small clusters due to the short-range (<5 Å) attraction and long-range repulsion characteristic of the Fe atoms on graphene [24,29], and the clusters may exhibit high spin polarization [30–32]. More importantly, when the surface coverage of Fe atoms on graphene was smaller than 55 %, the density of Fe islands on graphene was proportional to the coverage. This indicates that Fe clusters tend to exist independently at low coverage [29]. Therefore, further study of the unique properties of Fe clusters adsorbed onto graphene is of great significance.

* Corresponding authors at: School of Physics Science and Information Technology, Liaocheng University, Liaocheng 252000, China (X.-C. Wang). Department of Electrical and Computer Engineering, The University of North Carolina at Charlotte, Charlotte, NC 28223-0001, USA (Yong Zhang).
E-mail addresses: yong.zhang@uncc.edu (Y. Zhang), wangxiaochun@jlu.edu.cn (X.-C. Wang).

https://doi.org/10.1016/j.apsusc.2023.157315
Received 10 November 2022; Received in revised form 1 April 2023; Accepted 17 April 2023
Available online 20 April 2023

In recent years, the adsorption of Fe clusters on graphene has attracted considerable attention. Previous studies have mostly focused on the effects of single or two Fe atom adsorption [9,24,33,34]. The magnetic moment of the Fe_n ($n > 2$) clusters adsorbed on graphene is interesting. Johll *et al.* reported the stability and magnetic moment of Fe trimers and tetramers adsorbed on graphene [35]. Srivastava *et al.* studied the defect effect in graphene about the magnetism and bonding characteristics of Fe_n/graphene ($n = 1–5$) [25]. In addition, the structures and magnetism of Fe_n/graphene ($n = 2–7$) have been studied by Liu *et al.* [36]. In the Fe_n/graphene system, the most energetically favorable Fe_3 had a planar structure (2D). However, when $n \geq 4$, three-dimensional (3D) structure, such as tetrahedral Fe_4, appears to be energetically more favorable. Therefore, the Fe_4 cluster is the smallest 3D structure among all Fe_n clusters considered. Despite the configuration of the lowest energy Fe_4 cluster has been identified [36], the detailed properties of the Fe_4 cluster adsorption on graphene, particularly the charge exchange between the cluster and graphene, the diffusion barrier of Fe_4 between different sites on graphene, and the magnetic moment remain ambiguous, and the potential applications of the Fe_4/graphene system are yet to be explored.

In this study, Fe_4 clusters on graphene with different configurations and sites were systematically investigated. We paid special attention to the energy differences and diffusion barriers between different *meta*-stable states of the cluster, corresponding to different sites on graphene. These results provide insights into polyatomic adsorption and potential applications based on the nanoscale magnetic levitation (maglev) of the Fe-graphene system. Significantly, for this nano-maglev, it is the electrostatic force instead of the gravity in classic maglev to be balanced by the magnetic force [37].

2. Methods

The calculations were performed by applying the projector-augmented wave (PAW) pseudopotential method [38,39] based on the density functional theory (DFT) with the generalized gradient approximation (GGA) in the form of Perdew-Burke-Ernzerhof (PBE) [40] implemented in the VASP code [41,42]. The calculations were carried out using a $10 \times 10 \times 1$ graphene supercell with 15 Å vacuum layer and 600 eV energy cutoff. The calculated lattice constant of graphene is 2.46 A, which is in good agreement with previous reports [8,43]. A $1 \times 1 \times 1$ k-mesh was employed for the Brillouin zone integrations to relax the structures. For calculating the electronic properties of the Fe_4/graphene, the K-point was set as $2 \times 2 \times 1$. The total energy and the force of the optimized structure were converged to 1.0×10^{-5} eV and 0.01 eV/Å, respectively. The climbing image nudged elastic band (CI-NEB) method was used to calculate the diffusion energy barrier [44]. In view of the difficulty of calculating the convergence of the transition state, here we uniformly use 0.05 eV/Å and 1.0×10^{-5} eV as the convergence accuracy of force and energy, respectively. In addition, 5 images were inserted between 3D-H_2T_2 structure and 3D-B_3H to accurately describe the overpotential of its deformation. To correct the dispersion relationship, we used DFT-D3 to correct the van der Waals interaction. [45] The deformation between the remaining quantum states was small, so one image was inserted. Bader charge population analysis was adopted to describe electron transfer.[46–48] We employed *ab initio* molecular dynamics (AIMD) simulation at 300 K to test the thermal stability of the Fe_4/graphene system for the configuration (3D-B_3H). The 3D-B_3H structure with the NVT (for a system with constant number of particles (N), volume (V) and temperature (T)) canonical ensemble was used for the AIMD simulation, which lasted for 10 ps with time steps of 2.0 fs.

3. Results and discussion

3.1. Fe_4 cluster on graphene

The adsorption energy (E_{Ads}) was calculated to describe the thermodynamic stability by the following expression:

$$E_{Ads} = E_{sub+ads} - E_{sub} - E_{ads} \quad (1)$$

where $E_{sub+ads}$, E_{sub} and E_{ads} are the total energy of the Fe/graphene system, graphene and adsorbate, respectively. A negative value means that the Fe atom adsorption process is spontaneous.

Here, the four Fe atoms (Fe_4) are adsorbed on graphene in two general forms: 2D-parallelograms and 3D-tetrahedrons (in Fig. S1). The 2D Fe_4 clusters have three possible initial adsorption configurations, named as 2D-B (Fig. S1(a), Fe atoms on the bridge sites of graphene), 2D-T (Fig. S1(b), Fe atoms on the top sites), and 2D-H (Fig. S1(c), Fe atoms on hollow sites), respectively. Different from the 2D Fe_4 clusters on graphene, the 3D Fe_4 clusters in Fig. S1(d-i) are named with two letters. The first (second) letter specifies the sites of the Fe atoms in the bottom (top) layer of Fe_4 cluster, and the number subscripts indicate the number of Fe atoms on the relevant layer. There are 4 cone-like structures, as shown in Fig. S1(e) – (h). For example, in Fig. S1(e), the 3D-B_3H structure indicates that the adsorbed Fe_4 cluster has three Fe atoms in the first layer locating at the bridge sites of graphene, and one Fe atom in the second layer locating at the hollow site. After the structure optimization, Fig. 1(e) is obtained, and the first-layer Fe atoms deviate from the initial position. For convenience, we still use 3D-B_3H to name the state. Since single Fe atom is inclined to be adsorbed at the graphene hollow site [9,24], herein, for the apex adsorption configurations (an inverted cone), only the 3D-HT_3 configuration is considered (Fig. S1(d)). The optimized structures are shown in Fig. 1(a)-(h) and Fig. S1(j), where Fig. S1(j) is the optimized 3D-H_2T_2. For the 2D planar structures, the most stable configuration is 2D-H, which has the −0.845 eV E_{Ads}. As for the 3D cone-shape structures, the 3D-B_3H is the most stable configurations due to the lowest E_{Ads} −1.854 eV (only 91 meV higher than 3D-H_2T_2). The E_{Ads} values for other adsorption configurations are −0.426 eV for 2D-T, −0.429 eV for 2D-B, −1.442 eV for 3D-HT_3, −1.438 eV for 3D-T_3H, −1.431 eV for 3D-H_3T, and −1.253 eV for 3D-T_3T, respectively. Therefore, compared the 2D structures, Fe_4 cluster tern to formed 3D configuration on graphene. On the other hand, the van der Waals correction is important, so we added the van der Waals correction to compare the E_{Ads} of Fe_4 cluster on graphene with 3D structure. The E_{Ads} of 3D-H_2T_2, 3D-B_3H, 3D-H_3T, 3D-T_3H and 3D-T_3T is −1.619, −1.618, −1.209, −1.199 and −1.017 eV, respectively. Among these structures, Fig. S1(i), 3D- H_2T_2 (E_{Ads} = -1.619 eV) is the lowest energy adsorption configuration with one edge of the Fe tetrahedron laying across the carbon bond, same as that identified previously by Liu *et al.* [36]. Thus, 3D- H_2T_2 can be considered as the ground state of the Fe_4 cluster on graphene. The average Fe-Fe bond length in 3D- H_2T_2 is 2.31 Å, which is very close to 2.32 Å that reported by Johll *et al.* [35]. From the above results, we can find that Fe_4 clusters have multiple quantum states on graphene, and the difference in the adsorption energy of the quantum states is small. And 3D-B_3H is a representation of the 3D regular tetrahedral structure.

In order to further verify the accuracy and rationality of our calculations, we compared some landmark typical articles. For 3D-HT_3, our result of −1.144 eV is close to that of −1.209 eV from Srivastava *et al.* [25], both using the PBE pseudopotentials in VASP. Moreover, the magnetic moment for 3D-H_3T of our calculation is 9.78 μ_B, which is only 8 % smaller than the report of Liu *et al.* [36]. However, our results for 3D-H_3T (-1.209 eV) and 3D-T_3H (-1.199 eV) are rather different from those reported by Johll *et al.* (-0.96 eV for 3D-H_3T and −0.92 eV for 3D-T_3H) [35], which is likely due to the different choices of the software codes and pseudopotentials. However, the interactions between clusters and energy barriers for interconversion between different quantum states have not yet been studied in the work of Srivastava *et al.* We finish these studies, and find a new nanomagnetic levitation phenomenon, and further focus on the application value of Fe_4 clusters on graphene.

3D-H_2T_2 has the lowest energy state, and 3D-B_3H is representative of the adsorption configuration of a regular tetrahedron on graphene. The

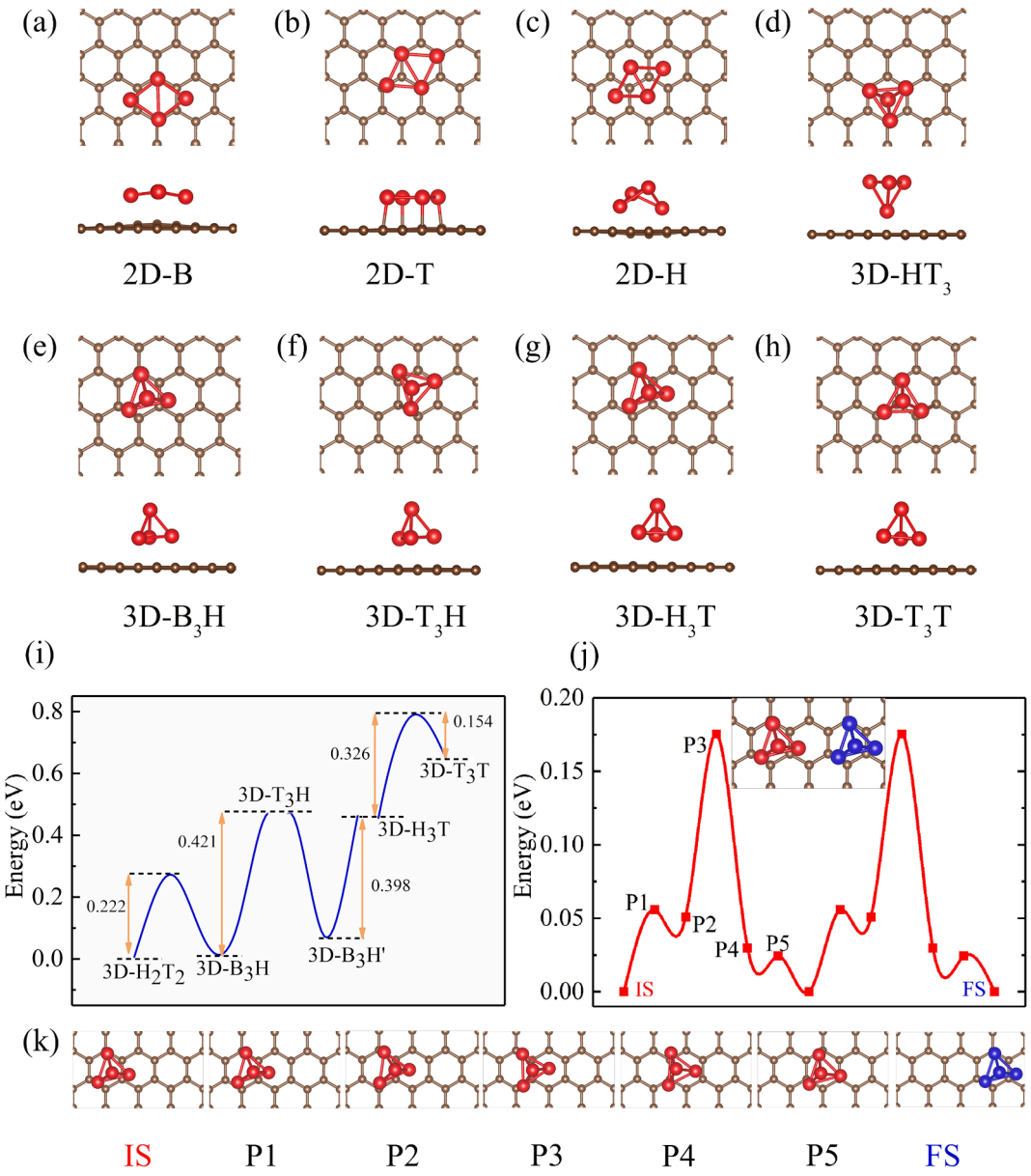

Fig. 1. (a-h) Top and side view of the optimized structures of Fe_4 clusters adsorbed on graphene. (i) The diffusion energy barriers between different 3D Fe_4 clusters. (j) Diffusion energy profile of the Fe_4 cluster on graphene with 3D-B_3H structure. (k) Real space diffusion path of the Fe_4 cluster for 3D-B_3H configuration in (j).

energy of 3D-H_2T_2 is only 0.001 eV lower than that of 3D-B_3H. To reveal the connection between 3D-H_2T_2 and 3D-B_3H, we calculated the energy barrier of the Fe_4/graphene system migrating from the 3D-H_2T_2 to 3D-B_3H (5 images were inserted), yielding 0.222 eV, as shown in Fig. S2. The diffusion energy barrier is conducive to certain applications of Fe_4/graphene system. For instance, 3D-H_2T_2 could be used as a standby state that is very stable; but it can be excited through a proper mean to enter a metastable state, such as 3D-B_3H or one of the other maglev quantum states. Interestingly, the Fe_4 cluster in 3D-B_3H can remain stable, because certain energy barriers need to be overcome. To verify the stability and the application potential of 3D-B_3H configuration, we verified its thermal stability at 300 K by performing an AIMD simulation over a time duration of 10 ps. The results showed that the free energy oscillated within a small range but did not change abruptly and maintained good structural integrity (Fig. S3). In more detail, the average Fe-Fe bond length (Fe1-Fe4, Fe2-Fe4 and Fe3-Fe4) in 3D-B_3H also presents a simple harmonic vibration rather than a sudden change (Fig. S4). This shows that during the simulation process, there was no abrupt deformation of the bond length of the Fe_4 cluster. In addition, during the simulation, 3D-B_3H 's energy variation interval was 0.21 % and the bond length variation was 15.22 %, which can be compared with the stable structure V_2N energy variation of 4.16 % and bond length variation of 33.33 % [49]. Compared with 3D-H_2T_2, 3D-B_3H has only one Fe atom at the top position, and the visible area of the quantum dot is smaller in 3D-B_3H. Therefore, the distance between the tips of adjacent quantum dots is larger in 3D-B_3H than 3D-H_2T_2, thus, it is easier to distinguish when detecting quantum dots in 3D-B_3H. Therefore, we chose 3D-B_3H as an example for detailed discussion. Therefore, we will focus our attention on the interesting states (3D-B_3H) of Fe_4/graphene that is the Fe_4 clusters on graphene in the 3D form of a cone-like tetrahedron.

To investigate the mobility of the Fe_4 cluster on graphene, we have calculated the diffusion energy barriers of the 3D Fe_4 cluster between different configurations on graphene using the CI-NEB method [44], as shown in Fig. 1(i). Here we take the fully relaxed structures of Fe_4/graphene as the beginning and end positons of CI-NEB to study, and discuss the energy barriers of transitions between the neighbouring different structures. The diffusion barriers of Fe_4 cluster on graphene between 3D-B_3H and 3D-T_3H, 3D-T_3H and 3D-H_3T, as well as 3D-H_3T

and 3D-T_3T are 0.419, −0.389 and 0.326 eV, respectively (one image was inserted).The structures of 3D-B_3H' can be obtain by slightly rotating the 3D-B_3H. 3D-B_3H is the most stable structure in the 3D cone-like structures, so the diffusion energy barrier of 3D-B_3H was studied. Moreover, the results in Fig. 1(j) offer an approximate description of the energy landscape for 3D Fe_4 moving on graphene starting from a 3D-B_3H site and ending at another equivalent (five images were inserted) site, which is relatively flat with the highest barrier of 0.175 eV, which is much smaller than the barrier for a single Fe of 0.4–0.5 eV [26]. The corresponding real space path is shown in Fig. 1(k). Besides, the energy variation is smaller than those in some energy storage 2D materials, such as a single atom of Li, Na and K diffusion on MoN_2 with a barrier of 0.78 eV, 0.56 eV and 0.49 eV, respectively [50]. It can be used for the charging and discharging processes. Therefore, we can analogize that the diffusion rate of Fe_4 clusters on graphene can be compared to or even surpassed by electron transfer. Moreover, according to an empirical reaction rule, when the reaction barrier is less than 0.91 eV/elementary-entity (21 kcal/mol), the migration can easily occur even at room temperature [51]. The calculated diffusion barrier of the Fe_4 cluster (3D-B_3H state) on graphene at 0 K is 0.175 eV/Fe_4, which is remarkably smaller than 0.91 eV/elementary-entity by 5 times. Such low diffusion barriers suggest excellent mobility of the 3D Fe_4 clusters on graphene. Nevertheless, without external stimuli, the Fe_4 cluster can remain stably at one site.

3.2. Magnetic moment induced by Fe_4 clusters

The magnetic property of materials is an important factor that affects the practical application of materials. Therefore, the magnetic moment of the Fe_4 cluster is studied by calculating the three-dimensional spin-density distributions of different configurations, as shown in Fig. S5. We take the structure 3D-B_3H as a representative to study the spin-density distributions (Fig. 2(a)). The bond lengths of the Fe4-Fe1, Fe4-Fe2 and Fe4-Fe3 atoms are 2.253 Å, 2.304 Å and 2.282 Å, respectively, which is highly consistent with previous reports [52]. The spin-up magnetic moment of the Fe4 atom (2.631 μ_B) is the highest among the Fe atoms in the 3D-B_3H structure, all of which are smaller than the average magnetic moment (3 μ_B) of Fe atom in a free 3D Fe_4 cluster [52]. As for graphene, the total magnetic moment of C atoms is −0.266 μ_B with spin-down, which can be mainly found under the Fe atoms, as shown in Fig. 2(b). Clearly, the direction of the magnetic moment in the Fe cluster is opposite to that of the C atoms in graphene. This interesting phenomenon is attributed to the unique adsorption of Fe_4 clusters on graphene. Here, we discuss in detail about the diamagnetic moment induced by the adsorption of the Fe_4 cluster on graphene. These spontaneous and opposite magnetic moments result in a repulsive effect, that weakens the bonding between the Fe_4 cluster and graphene, resulting in a modest diffusion energy barrier. Thus, the Fe_4 cluster may serve as a miniature maglev object on graphene with interesting potential applications in nano-devices.

To gain a better understanding of the electron transfer between Fe_4 cluster and graphene, the change of the electron density $\Delta\rho_1$ is calculated, which is defined as:

$$\Delta\rho 1 = \rho_{sub+ads} - \rho_{sub} - \rho_{ads} \quad (2)$$

where $\rho_{sub+ads}$, ρ_{sub} and ρ_{ads} are the charge density of the Fe_4/graphene system, the graphene and the Fe_4 cluster in the final configuration, respectively. The $\Delta\rho_1$ accounts for the charge redistribution caused by the interaction between Fe_4 and graphene. Bader charge analysis shows that the 0.956 electrons are transferred from the Fe_4 cluster to graphene, which leads to electron redistribution in Fe_4/graphene system, as shown in Fig. 2(c). The slightly different of the charge and the magnetic moment of the Fe atoms in 3D-B_3H structure are caused by the spontaneous symmetry breaking principle, which leads to the charge redistribution of the four Fe atoms (-0.336 e, −0.309 e, −0.355 e, and 0.044 e for Fe1, Fe2, Fe3 and Fe4, respectively, compared with free Fe atoms). Additionally, a large amount of charge accumulates at the space

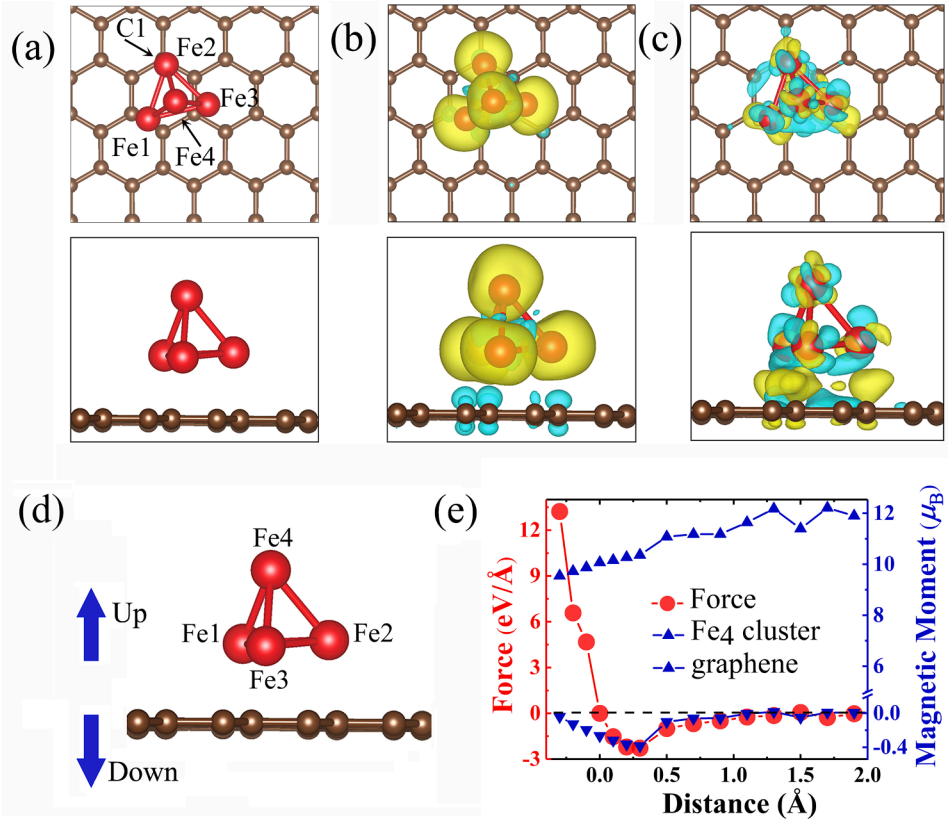

Fig. 2. (a) The configuration of the 3D-B_3H cluster. (b) Three-dimensional spin-density distribution, where the yellow isosurface represents the spin up density. (c) The electron density difference, where the yellow and blue represent electron accumulation and depletion, respectively. The isovalue is 0.005 e/Å^3. (d) The schematic diagram of the repulsive force between the Fe_4 cluster and graphene. (e) The force exerted on Fe_4 cluster, and the magnetic moment of Fe_4 cluster and graphene change with the distance. The distance between Fe_4 and graphene for equilibrium Fe_4/graphene is set to 0 Å. (For interpretation of the references to colour in this figure legend, the reader is referred to the web version of this article.)

between the Fe_4 cluster and the graphene surface, indicating that there is a strong interaction between them. Moreover, the electron charge transferred from the Fe_4 cluster results in electron redistribution in graphene, and further modifies the unpaired electrons of C atoms. Some spin-up *p* orbital electrons of C atoms transfer to the area between graphene and the Fe_4 cluster, forming an electronic buffer layer. Electron depletion (on the upper side of graphene) and electron accumulation (on the lower side of graphene) break the balance between the spin-up and spin-down *p* orbital electrons of C atoms beneath the Fe_4 cluster, inducing the diamagnetic moment of C atoms. Our analysis indicates that the change of the magnetic moment of Fe atom is due to the transfer of its electrons from Fe cluster to graphene, leading to the electron redistribution of the system, rather than the transfer of Fe electrons from *s* orbital to *d* orbital [9][].

From another point of view, the adsorption state of Fe_4 clusters on graphene is very important and will determine its application prospects. Therefore, we study the force between Fe_4 clusters and graphene. The force of graphene exerting on the Fe_4 cluster is explored by moving the Fe_4 cluster up-and-down, as shown in Fig. 2(d) and (e). The stable position 3D-B_3H is set as the reference point for both force and distance. When the distance between the Fe_4 cluster and the graphene is greater than the equilibrium value, the Fe_4 cluster is attracted to graphene. Conversely, the Fe_4 cluster is repulsed by graphene. The repulsive force increases sharply as the distance decreases. On the other hand, the force exerted on the Fe_4 cluster of 3D-B_3H structure in the state without considering the magnetism was also calculated. Specifically, when the 3D-B_3H configuration is non-magnetic (ISPIN = 1), the equilibrium position of the Fe_4 cluster is at 1.978 Å above graphene; in contrary, the Fe_4 cluster can be stably suspended on graphene at 2.000 Å when the ISPIN = 2. Moreover, the optimized magnetic structure is subjected to static processing (ISPIN = 1), the Fe_4 cluster receives a downward electrostatic force (3.15 eV/Å) from graphene. For the magnetism of the Fe/graphene system, the magnetic repulsion between the Fe_4 cluster and graphene due to diamagnetism offsets the electrostatic interaction between them. When the relative distance is larger than the equilibrium value, the magnetic moments of Fe_4 increase and the diamagnetism of graphene decreases. The magnetic force levitates the Fe_4 cluster (repelling), but the change in the magnetic moment is small with varying distance. More interestingly, the magnitude of the electrostatic force changes, and the trend is to repel at a smaller distance and attract at a larger distance. Eventually, the magnetic repulsion and electrostatic attraction reach a balance. Therefore, the change in the force between the Fe_4 cluster and graphene is mainly due to the change in the electrostatic force.

To gain more insights into the origin of the aforementioned magnetism, the total density of states (TDOS) and the projected DOS (PDOS) of the 3D-B_3H structure are calculated. Fig. 3(a) shows that spin polarization appears at the Fermi level mainly originating from the Fe atoms, and C atoms contribute a small part. In Fig. 3(b-e), the PDOS of Fe atoms show that there is no obvious spin density found in the *s* and *p* orbitals, and the *d*-electron orbital mainly contributes to the TDOS and shows a remarkable spin splitting. We further explore the source of the magnetic moment of the C1 atom, which forms an Fe-C bond with the Fe_4 cluster. The electrons of the Fe_4 cluster and the substrate graphene are redistributed because of the Fe-C bonds, so the *p* orbital of C1 atom has unpaired electron, leading to the spin splitting in the PDOS of C1 atoms, as shown in Fig. 3(f). Moreover, we also calculated the PDOS of the remaining 3D structures (Fig. S6). It is clear that all Fe_4/graphene systems are metallic, and the asymmetric distribution of the exit density of states at the Fermi level is mainly caused by the *d*-electron spin splitting of Fe atoms. This result was consistent with the above discussion on the 3D-B_3H structure.

3.3. Potential applications in nano-devices

It is necessary to find the smallest super cell in which the neighboring Fe_4 clusters do not affect each other. The Fe_4 clusters on different supercell size of graphene was studied. As shown in Fig. 4, the total

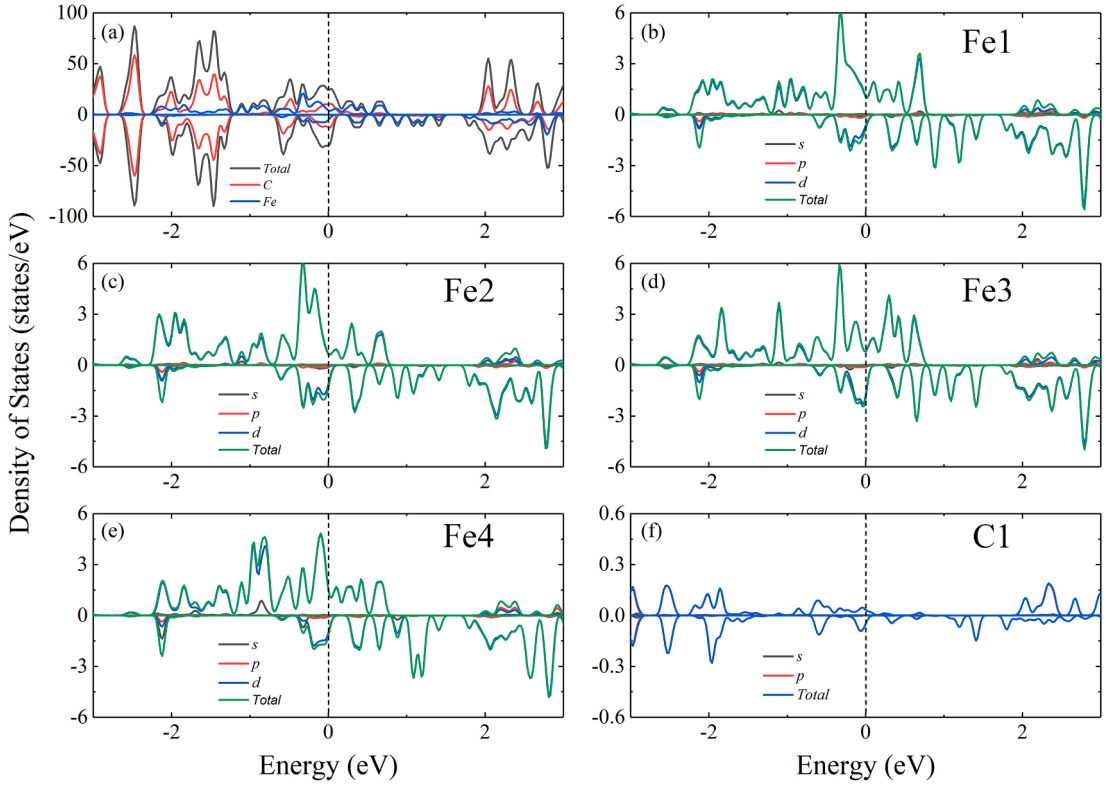

Fig. 3. The density of states of the 3D-B_3H structure. The total spin density of states and partial density of states for 3D-B_3H (a) and for the representative atoms Fe1 atom (b), Fe2 atom (c), Fe3 atom (d), Fe4 atom (e) and C1 atom (f). The Fermi level is set to zero. C1, Fe1, Fe2, Fe3 and Fe4 atoms are shown in Fig. 2(a).

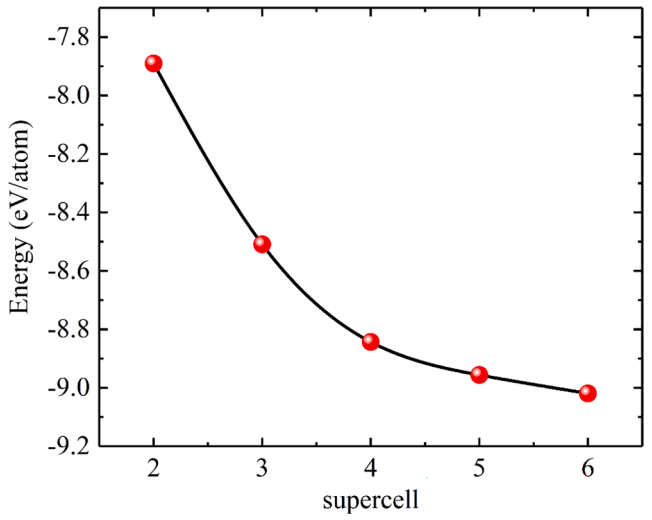

Fig. 4. The energy per atom of Fe_4/graphene system at different sizes graphene.

energy per atom decrease with increasing supercell size (from 2 × 2 to 6 × 6). From the 2 × 2 to 3 × 3 super cell, the total energy per atom reduces by 7 %. The total energy per atom of the 4 × 4 graphene supercell is −8.89 eV/atom that is 4 % lower than −8.56 eV/atom of the 3 × 3 graphene super cell. From 4 × 4 to 5 × 5 supercell, only 1 % energy difference is observed. Additionally, the structure of the Fe_4 clusters with the 4 × 4 (5 × 5) supercells is consistent with that of 3D-B_3H (Fig. S7 (a-c)). Therefore, we expect that the change will be negligible beyond 4 × 4.

To further uncover the Fe clusters interactions, Fig. S7 (d-f) show the calculated deformation charge density difference ($\Delta\rho_2$), which is defined as:

$$\Delta\rho 2 = \rho_{sub+ads} - \sum_{\mu}\rho_{atom}(\vec{r} - \overrightarrow{R_{\mu}}) \quad (3)$$

It reflects the difference between the adsorbed Fe_4/graphene system and the charge density superposition of each atom. 1.232 electrons are transferred from the Fe_4 cluster to the graphene in 3 × 3 super cell, and the height of Fe clusters from the substrate is only 1.563 Å. This indicates that the Fe_4 clusters have stronger interactions with the substrate, thus leading to obvious deformation of the graphene substrate, as shown in Fig. S7(d). However, Fe_4 clusters lose less electrons on the 4 × 4 supercell (0.866 e), and the 1.896 Å height of Fe_4 cluster in 4 × 4 supercell is greater than that 1.563 Å of 3 × 3 supercell, which means that the interaction between Fe clusters and graphene is reduced. Moreover, the deformation effects vanish in the 4 × 4 supercell (Fig. S7 (e)). It reveals that the direct interactions between the adjacent Fe_4 clusters have become minimal for the 4 × 4 supercell. On the other hand, the magnetic moment of the Fe atom in the 4 × 4 supercell is closer to that of 3D-B_3H rather than in the 3 × 3 supercell (Table S1). This also suggests that the 4 × 4 graphene supercell can be used as the minimal unit for the nearly independent Fe_4 clusters.

The trend of decreasing total energy per atom with increasing graphene size implies that the Fe_4 clusters tend to repel each other instead of aggregating into a larger cluster, which is consistent with the finding that the Fe islands prefer to grow in 3D instead of coarsening laterally [9]. This conclusion is also supported by the experimental finding of Binz *et al.* [29]. When the distance between Fe adatoms is greater than 0.5 nm, there is a repulsive interaction. The lateral distance between the Fe_4 cluster on the 4 × 4 graphene supercell is 0.99 nm, and this distance allows the Fe clusters to maintain the most stable cone-like configuration (3D-B_3H), so the Fe_4 clusters may exist independently in the 4 × 4 graphene supercell. Thereby, in the 4 × 4 super cell, individual 3D Fe_4 clusters can be viewed as an independent quantum dot array with the maximum density around $1.18 \times 10^{14}/cm^2$ on graphene.

The above studies have proved that Fe_4 clusters form a high-density arrangement on graphene with 4 × 4 super cell as the unit. And it can be suspended on graphene by magnetic repulsive interactions. Here, we further discuss the difference between quantum magnetic levitation and classical interaction force. The basic requirement for the classical maglev of an object is that the gravity and magnetic force are in balance. However, for the quantum magnetic levitation, it is the cancellation of electrostatic force and magnetic force, as in the case considered here. The Fe_4 cluster has a gravity force of $3.71x10^{-24}$N, which is far smaller than the electrostatic interaction force 5.04×10^{-9}N (3.15 eV/Å) by 10^{15} in magnitude. Therefore, the classical maglev principle is not suitable for quantum maglev applications.

It has been suggested that the development direction of the future generation of smaller maglev particles should meet three basic requirements: the stronger magnetic field, smaller equipment in size (reduce the distance of movement) and operating at lower temperature [37]. According to our results, the Fe_4/graphene system has shown excellent talent as a kind of nano-maglev. Firstly, at the nanoscale, graphene is a bumpy surface for the maglev particle Fe_4 with "valleys" and "hills". The "valleys" of different depths can serve as different quantum states, whereas the "hills" preserve these *meta*-stable states before an external perturbation is applied to alter them. These properties suggest potential applications in quantum or neuromorphic computing, such as providing multi-state memory units with an ultra-high density ($\sim 10^{14}/cm^2$ for the 4 × 4 structure). The more details introduction is shown in SM. Our work further explores and advances the application of high-density Fe clusters in spintronics or computer storage media [29]. Secondly, the modest energy barriers between different states are 0.419 eV for 3D-B_3H/3D-T_3H, 0.222 eV for 3D-H_2T_2/3D-B_3H, 0.325 eV for 3D-H_3T/3D-T_3T, as shown in Fig. 1(i). Significantly, the Fe_4 cluster has an ultra-low diffusion energy barrier (0.175 eV/Fe_4) between equivalent sites or the same state on different sites on graphene, which might be of interest for certain applications requiring a large lateral motion of the particle. In contrast to the superconducting based maglev that requires low-temperature operation, the Fe_4/graphene system can work at room temperature. Additionally, the Fe_4 cluster has a higher magnetic moment (the average magnetic moment > 2.5 μ_B/atom) than the Co_4 cluster (the average magnetic moment < 0.5 μ_B/atom) and Ni_4 cluster (the average magnetic moment < 2 μ_B/atom) [35]. Larger size clusters ($n \geq 5$) might have stronger magnetic moments, but they are expected to have lower energy barriers between different states and will reduce the maximum usable cluster density. In conclusion, with Fe_4 being the smallest 3D cluster (In Fe_n clusters), we believe that Fe_4/graphene is an optimal choices for the quantum maglev particles.

4. Conclusions

In this work, the adsorption energies, diffusion energy barriers, and magnetism of Fe_4 clusters on graphene were investigated using first-principles calculations. The charge transferred from the Fe_4 cluster to graphene raises a diamagnetic moment in graphene, which is the opposite of that of the Fe_4 cluster. The 3D Fe_4 clusters in different adsorption configurations exhibit small differences in adsorption energy and modest diffusion barriers, which make them diffusible between different sites with a minimal lateral force and remain stable against thermal fluctuation. The low diffusion energy barrier of the Fe_4 cluster is due to the spontaneous magnetic repulsion between the Fe_4 cluster and graphene. With the smallest 3D maglev particle Fe_4 in Fe_n/graphene, the Fe_4/graphene system may have a number of important applications. Due to the modest transition barriers, the transitions between the different quantum states of the Fe_4 cluster requires less energy; thus, they can potentially be used for energy-efficient, ultra-high-density data storage devices with multi-level quantum bits. Furthermore, the Fe_4/graphene system alleviates the low temperature requirement of magnetic

levitation and can be used for nanoscale maglev devices, such as an ultrasensitive force and inertial sensor. Flexible linear accelerometer is one of the typical representations of inertial sensor. Fe_4/graphene can be used as flexible linear accelerometer. When the Fe_4/graphene system accelerates, Fe_4 can change its quantum state under the influence of weak inertial force (From one state to another state, it can stay at later state unless force in the opposite direction is applied, so it is flexible.), showing whether there is inertia. Therefore, it can be used as an ultrasensitive flexible linear accelerometer. This study removes the dependence of magnetic levitation on superconducting materials and provides new options for developing magnetic levitation applications.

CRediT authorship contribution statement

Ning-Gui Ma: Conceptualization, Methodology, Software, Investigation, Formal analysis, Writing – original draft. **Yong-Jia Zhang:** Validation, Writing – review & editing. **He-Na Zhang:** Validation. **Hui-Min Mu:** Validation. **Yong Zhang:** Supervision, Formal analysis, Writing – review & editing. **Xiao-Chun Wang:** Writing – review & editing, Resources, Supervision, Funding acquisition.

Declaration of Competing Interest

The authors declare that they have no known competing financial interests or personal relationships that could have appeared to influence the work reported in this paper.

Data availability

Data will be made available on request.

Acknowledgements

This work was supported by the National Natural Science Foundation of China (Grant no. 11474123). YZ acknowledge the support of Bissell Distinguished Professor endowment at UNC-Charlotte.

Appendix A. Supplementary material

Supplementary data to this article can be found online at https://doi.org/10.1016/j.apsusc.2023.157315.

References

[1] K.S. Novoselov, A.K. Geim, S.V. Morozov, D. Jiang, Y. Zhang, S.V. Dubonos, I. V. Grigorieva, A.A. Firsov, Electric field effect in atomically thin carbon films, Science 306 (2004) 666–669.
[2] A.K.G. K.S. Novoselov, S.V. Morozov, D. Jiang, M.I. Katsnelson, I.V. Grigorieva, S. V., A.A.F. 22 Dubonos two-dimensional gas of massless dirac fermions in graphene, Nature, 438 (2005) 197–200.
[3] J.C. Meyer, A.K. Geim, M.I. Katsnelson, K.S. Novoselov, T.J. Booth, S. Roth, The structure of suspended graphene sheets, Nature 446 (2007) 60.
[4] L.-L. Liu, Y. Wang, C.-P. Chen, H.-X. Yu, L.-S. Zhao, X.-C. Wang, Tuning the electronic and magnetic properties of penta-graphene using a hydrogen atom: a theoretical study, RSC Adv. 7 (2017) 40200–40207.
[5] L.-L. Liu, C.-P. Chen, L.-S. Zhao, Y. Wang, X.-C. Wang, Metal-embedded nitrogen-doped graphene for H2O molecule dissociation, Carbon 115 (2017) 773–780.
[6] X. Chen, L. Xu, L.-L. Liu, L.-S. Zhao, C.-P. Chen, Y. Zhang, X.-C. Wang, Adsorption of formaldehyde molecule on the pristine and transition metal doped graphene: First-principles study, Appl. Surf. Sci. 396 (2017) 1020–1025.
[7] X.-C. Wang, Y. Zhang, F.-C. Liu, Y. Ma, W. Feng, S.-X.-A. Zhang, Dynamic nano-pulling effect of the boron-functionalized graphene monovacancy for molecule dissociation, J. Phys. D Appl. Phys. 46 (2013), 385302.
[8] W. Zhang, W.-C. Lu, H.-X. Zhang, K.-M. Ho, C.-Z. Wang, Hydrogen adatom interaction on graphene: A first principles study, Carbon 131 (2018) 137–141.
[9] X. Liu, C.Z. Wang, Y.X. Yao, W.C. Lu, M. Hupalo, M.C. Tringides, K.M. Ho, Bonding and charge transfer by metal adatom adsorption on graphene, Phys. Rev. B 83 (2011), 235411.
[10] X. Liu, C.Z. Wang, M. Hupalo, Y.X. Yao, M.C. Tringides, W.C. Lu, K.M. Ho, Adsorption and growth morphology of rare-earth metals on graphene studied by ab initio calculations and scanning tunneling microscopy, Phys. Rev. B 82 (2010), 245408.
[11] M. Hupalo, X. Liu, C.Z. Wang, W.C. Lu, Y.X. Yao, K.M. Ho, M.C. Tringides, Metal nanostructure formation on graphene: Weak versus strong bonding, Adv. Mater. 23 (2011) 2082–2087.
[12] M. Hupalo, S. Binz, M. Tringides, Strong metal adatom–substrate interaction of Gd and Fe with graphene, J. Phys. Condens. Matter 23 (2011), 045005.
[13] Z. Alisultanov, Electronic states of monatomic layers of alkali and rare earth metals adsorbed on graphene surfaces, Low Temp. Phys. 39 (2013) 172–179.
[14] E.E. Helgee, A. Isacsson, Adsorption of metal atoms at a buckled graphene grain boundary using model potentials, AIP Adv. 6 (2016) 1530.
[15] W. Liu, C. Zhang, M. Deng, S. Cai, The structural and electronic properties of metal atoms adsorbed on graphene, Physica E 93 (2017) 265–270.
[16] E. Olsson, G. Chai, M. Dove, Q. Cai, Adsorption and migration of alkali metals (Li, Na, and K) on pristine and defective graphene surfaces, Nanoscale 11 (2019) 5274–5284.
[17] V.V. Chi, Z. Kassirbodon, H. Yang, J. Coraux, J. Vogel, S. Pizzini, P. Bayleguillemaud, M. Chshiev, L. Ranno, V. Santonacci, Perpendicular anisotropy of ultrathin epitaxial cobalt films on graphene, New J. Phys. 12 (2010), 103040.
[18] G. Yu, M. Zhu, Y. Zheng, First-principles study of 3d transition metal atom adsorption onto graphene: The role of the extended line defect, J. Mater. Chem. C 2 (2014) 9767–9774.
[19] H.K. Dong, Y.P. Wang, L.B. Shi, First principles study of HCN adsorption on graphene doped with 5D transition metal, Surf. Rev. Lett. 23 (2016) 20190-.
[20] E. del Castillo, F. Cargnoni, R. Soave, M.I. Trioni, Spin-polarized charge transfer induced by transition metal adsorption on graphene, Phys. Scr. 91 (2016), 053007.
[21] P. Kratzer, S.A. Tawfik, X.Y. Cui, C. Stampfl, Detection of adsorbed transition-metal porphyrins by spin-dependent conductance of graphene nanoribbon, RSC Adv. 7 (2017) 29112–29121.
[22] G.X. Chen, H.F. Li, X. Yang, J.Q. Wen, Q. Pang, J.M. Zhang, Adsorption of 3d transition metal atoms on graphene-like gallium nitride monolayer: A first-principles study, Superlattice. Microst. 115 (2018) 108–115.
[23] H. Valencia, A. Gil, G. Frapper, Trends in the adsorption of 3d transition metal atoms onto graphene and nanotube surfaces: a DFT study and molecular orbital analysis, J. Phys. Chem. C 114 (2010) 14141–14153.
[24] X. Liu, C.Z. Wang, M. Hupalo, W.-C. Lu, P.A. Thiel, K.M. Ho, M.C. Tringides, Fe-Fe adatom interaction and growth morphology on graphene, Phys. Rev. B 84 (2011).
[25] M.K. Srivastava, Y. Wang, A.F. Kemper, H.-P. Cheng, Density functional study of gold and iron clusters on perfect and defected graphene, Phys. Rev. B 85 (2012) 165444.
[26] C.D. Porter, D. Stroud, Clustering and magnetic anisotropy of Fe adatoms on graphene, Phys. Rev. B 85 (2012), 235452.
[27] H. Sevinçli, M. Topsakal, E. Durgun, S. Ciraci, Electronic and magnetic properties of 3d transition-metal atom adsorbed graphene and graphene nanoribbons, Phys. Rev. B 77 (2008), 195434.
[28] I. Suarez-Martinez, A. Felten, J.J. Pireaux, C. Bittencourt, C.P. Ewels, Transition metal deposition on graphene and carbon nanotubes, J. Nanosci. Nanotechnol. 9 (2009) 6171–6175.
[29] S.M. Binz, M. Hupalo, X. Liu, C.Z. Wang, W.C. Lu, P.A. Thiel, K.M. Ho, E.H. Conrad, M.C. Tringides, High island densities and long range repulsive interactions: Fe on epitaxial graphene, Phys. Rev. Lett. 109 (2012), 026103.
[30] S.B. Fagan, R. Mota, A.J.R. da Silva, A. Fazzio, Ab initiostudy of an iron atom interacting with single-wall carbon nanotubes, Phys. Rev. B 67 (2003), 205414.
[31] S.B. Fagan, R. Mota, A.J.R. da Silva, A. Fazzio, Electronic and magnetic properties of iron chains on carbon nanotubes, Microelectron. J. 34 (2003) 481–484.
[32] Y. Zhang, N.W. Franklin, R.J. Chen, H. Dai, Metal coating on suspended carbon nanotubes and its implication to metal–tube interaction, Chem. Phys. Lett. 331 (2000) 35–41.
[33] Y. Mao, J. Yuan, J. Zhong, Density functional calculation of transition metal adatom adsorption on graphene, J Phys Condens Matter 20 (2008), 115209.
[34] H. Johll, H.C. Kang, E.S. Tok, Density functional theory study of Fe Co, and Ni adatoms and dimers adsorbed on graphene, Phys. Rev. B 79 (2009) 245416.
[35] H. Johll, J. Wu, S.W. Ong, H.C. Kang, E.S. Tok, Graphene-adsorbed Fe Co, and Ni trimers and tetramers: Structure, stability, and magnetic moment, Phys. Rev. B 83 (2011) 205408.
[36] X. Liu, C.-Z. Wang, H.-Q. Lin, M. Hupalo, P.A. Thiel, K.-M. Ho, M.C. Tringides, Structures and magnetic properties of Fe clusters on graphene, Phys. Rev. B 90 (2014) 155444.
[37] S. Ge, A. Nemiroski, K.A. Mirica, C.R. Mace, J.W. Hennek, A.A. Kumar, G. M. Whitesides, Magnetic Levitation in Chemistry, Materials Science, and Biochemistry, Angew. Chem. Int. Ed. Engl. 59 (2020) 17810–17855.
[38] P.E. Blochl, Projector augmented-wave method, Phys. Rev. B, Condensed Matter 50 (1994) 17953–17979.
[39] G. Kresse, D. Joubert, From ultrasoft pseudopotentials to the projector augmented-wave method, Phys. Rev. B 59 (1999) 1758.
[40] J.P. Perdew, K. Burke, M. Ernzerhof, Generalized gradient approximation made simple, Phys. Rev. Lett. 77 (1996) 3865.
[41] G. Kresse, J. Hafner, Ab initio molecular dynamics for liquid metals, Phys. Rev. B 47 (1993) 558.
[42] G. Kresse, J. Furthmüller, Efficient iterative schemes for ab initio total-energy calculations using a plane-wave basis set, Phys. Rev. B 54 (1996) 11169–11186.
[43] Y. Zhang, R. Tsu, Binding graphene sheets together using silicon: graphene/silicon superlattice, Nanoscale Res Lett 5 (2010) 805–808.
[44] G. Henkelman, B.P. Uberuaga, H. Jónsson, A climbing image nudged elastic band method for finding saddle points and minimum energy paths, J. Chem. Phys. 113 (2000) 9901–9904.
[45] J. Moellmann, S. Grimme, DFT-D3 Study of Some Molecular Crystals, J. Phys. Chem. C 118 (2014) 7615–7621.

[46] G. Henkelman, A. Arnaldsson, H. Jónsson, A fast and robust algorithm for Bader decomposition of charge density, Comput. Mater. Sci 36 (2006) 354–360.
[47] E. Sanville, S.D. Kenny, R. Smith, G. Henkelman, Improved grid-based algorithm for Bader charge allocation, J. Comput. Chem. 28 (2007) 899–908.
[48] R.F. Bader, A quantum theory of molecular structure and its applications, Chem. Rev. 91 (1991) 893–928.
[49] X. Zhao, P. Wang, E. Lv, C. Wu, K. Ma, Z. Gao, I.D. Gates, W. Yang, Screening MXenes for novel anode material of lithium-ion batteries with high capacity and stability: A DFT calculation, Appl. Surf. Sci. 569 (2021) 151050.
[50] X. Zhang, Z. Yu, S.-S. Wang, S. Guan, H.Y. Yang, Y. Yao, S.A. Yang, Theoretical prediction of MoN 2 monolayer as a high capacity electrode material for metal ion batteries, J. Mater. Chem. A 4 (2016) 15224–15231.
[51] D.C. Young, A practical guide for applying techniques to real-world problems, WileyeInterscience, New York, 2001.
[52] E. Kim, A. Mohrland, P.F. Weck, T. Pang, K.R. Czerwinski, D. Tománek, Magic numbers in small iron clusters: A first-principles study, Chem. Phys. Lett. 613 (2014) 59–63.